Applied Catalysis B: Environmental 180 (2016) 255–262

Contents lists available at ScienceDirect

Applied Catalysis B: Environmental

journal homepage: www.elsevier.com/locate/apcatb

(Au@Ag)@Au double shell nanoparticles loaded on rutile TiO_2 for photocatalytic decomposition of 2-propanol under visible light irradiation

Sunao Kamimura[a,b], Takeshi Miyazaki[a], Ming Zhang[c], Yuqing Li[c], Toshiki Tsubota[a], Teruhisa Ohno[a,b,d,*]

[a] Department of Applied Chemistry, Faculty of Engineering, Kyushu Institute of Technology, 1-1 Sensuicho, Tobata, Kitakyushu 804-8550, Japan
[b] Research Center for Advanced Eco-fitting Technology, Kyushu Institute of Technology, 1-1 Sensuicho, Tobata, Kitakyushu 804-8550, Japan
[c] School of Chemistry and Chemical Engineering, Yangzhou University, 88 South University Ave., Yangzhou, Jiangsu 225009, China
[d] ACT-C, Japan Science and Technology Agency, 4-1-8 Honcho, Kawaguchi-shi, Saitama 322-0012, Japan

ARTICLE INFO

Article history:
Received 14 May 2015
Received in revised form 15 June 2015
Accepted 17 June 2015
Available online 23 June 2015

Keywords:
Photocatalyst
Titanium oxide
Visible light-responsive photocatalyst
Localized surface plasmon resonance

ABSTRACT

We synthesized (core@shell)@shell ((Au@Ag)@Au) nanoparticles (NPs) by a multistep citrate reduction method for utilization as photosensitizers of TiO_2. The (Au@Ag)@Au NPs exhibited strong photoabsorption in visible light response due to LSPR excitation of the Ag shell, and its LSPR characteristics were stable under visible light irradiation for a long time because oxidation of the Ag shell was prevented by the outermost Au shell. Furthermore, we successfully loaded (Au@Ag)@Au NPs on rutile TiO_2 by an impregnation method. (Au@Ag)@Au/TiO_2 could oxidize 2-propanol into acetone and CO_2 under visible light irradiation ($\lambda > 440$ nm), and its acetone evolution rate was approximately 15-times higher than that of Au/TiO_2. From a comparison of action spectra for acetone evolution and the Kubelka–Munk function, it was confirmed that photocatalytic activity of (Au@Ag)@Au/TiO_2 was induced by photoabsorption based on LSPR excitation of the Ag shell. In addition, photoelectrochemical measurements revealed electron injection from LSPR-excited (Au@Ag)@Au NPs into TiO_2 under visible light irradiation. We proposed the photocatalytic reaction process of (Au@Ag)@Au/TiO_2 in conjunction with optical, structural and photoelectrochemical properties.

© 2015 Elsevier B.V. All rights reserved.

1. Introduction

Since the discovery of photoelectrochemical splitting of water on titanium dioxide (TiO_2) electrodes [1], TiO_2 has been intensively studied for its photocatalytic activity, which can be used to convert light energy to storable chemical fuels, or to address environmental issues such as treatment of waste water and cleaning of exterior windows by degradation of organic molecules [2–5]. TiO_2 displays photocatalytic activity only when irradiated by ultraviolet (UV) light because of its large band gap (~3.0 eV for rutile and 3.2 eV for anatase) [6]. A solar irradiance spectrum contains approximately 4% UV light, with visible light accounting for 50% and infrared light accounting for the remaining 46%. Therefore, the development of visible light-responsive TiO_2 is needed for expanding applications utilizing solar light as well as fluorescent lamps, incandescent lamps and light-emitting diodes.

Many approaches to develop visible light-responsive TiO_2 includings chemical doping and photosensitization have been proposed [7–10]. Chemical doping is the most common approach for narrowing the bandgap of TiO_2, while doped-ions in TiO_2 act as recombination centers for photo-excited electrons and holes, resulting in a decrease of photocatalytic activity [11]. Photosensitization of TiO_2 with organic dyes still presents major limitations for applications as a photocatalyst because of the poor stability of the dye, which can undergo desorption, photolysis and oxidative degradation, and fast back electron transfer, which results in low quantum yield for the photocatalytic reaction [12,13]. As an alternative to organic dyes, metallic nanoparticles (NPs) have been successfully used as photosensitizers for TiO_2 due to their stability and strong photoabsorption under visible light based on localized surface plasmon resonance (LSPR). Here the LSPR is coherent oscillation of electrons on the surfaces of the metallic NPs upon incident light irradiation. LSPR-induced photocatalytic activity of

* Corresponding author.
E-mail address: tohno@che.kyutech.ac.jp (T. Ohno).

http://dx.doi.org/10.1016/j.apcatb.2015.06.037
0926-3373/© 2015 Elsevier B.V. All rights reserved.

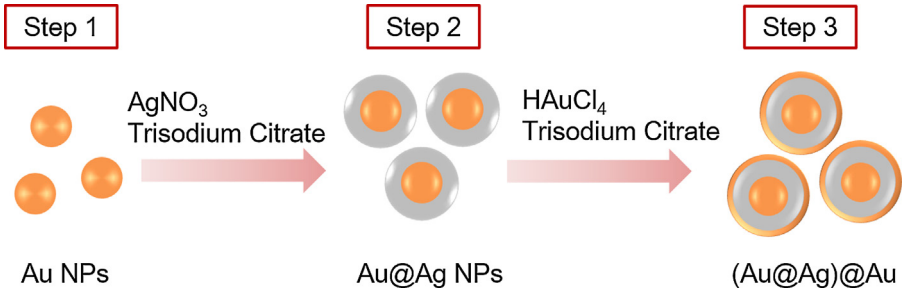

Scheme1. Synthesis procedure for (Au@Ag)Au NPs.

TiO_2 was first described in 2005 by Tatsuma et al. who found that gold (Au) NPs loaded on TiO_2 (Au/TiO_2) films can photocatalytically oxidize ethanol and methanol at the expense of oxygen reduction under visible light [14]. Kowalska et al. further investigated the photocatalytic decomposition of 2-propanol by utilizing Au/TiO_2 powders, and they proposed the following LSPR-induced photocatalytic reaction process: (1) Incident photons are absorbed by the Au NPs through thier LSPR excitation, (2) electrons in the Au NPs are injected into the conduction band of TiO_2, and (3) the resultant electron-deficient Au NPs can oxidize 2-propanol to be recovered to the original metallic Au NPs state [15]. There have been many reports concerning the photocatalytic activity of Au/TiO_2 and its mechanism [16–19].

Silver (Ag) NPs also display strong photoabsorption in the visible light range based on LSPR, and Ag/TiO_2 shows a higher incident-photon-to-current efficiency than that of Au/TiO_2 under irradiation of visible light [20]. However, Ag NPs have severe susceptibility to oxidation; that is, Ag NPs are oxidized at the interface between Ag and TiO_2, leading to the formation of silver oxide [21]. The oxidation of Ag gives rise to a decrease in the photoabsorption intensity and a shift in the LSPR wavelength [22,23]. Therefore, if oxidation of Ag NPs on TiO_2 can be prevented, it is expected that TiO_2 will achieve and maintain a high level of photocatalytic activity under visible light irradiation. Despite the multitude of attempts to synthesize aqueous core@shell structure, Ag@Au NPs, the challenges associated with synthesizing Ag@Au particles primarily stem from the galvanic replacement reaction that occurs between aqueous Au and metallic Ag during the shell deposition procedure. To synthesize monodispersed Ag@Au NPs, the galvanic replacement reaction should be suppressed or eliminated, which is a challenge. The present research was carried out from this standpoint. Our attention is now focused on the (core@shell)@shell structure, (Au@Ag)@Au NPs, where core Au and outermost Au shell provide electrons to the Ag shell for prevention of Ag oxidation [24]. The double shell structure (Au@Ag)@Au NPs were first revealed by Maenosono et al. for use as probes in sensing and biodiagnostics applications, and they showed that (Au@Ag)@Au NPs exhibited photoabsorption in the visible light range based on LSPR of the middle Ag shell [25]. However, the photocatalytic activity of (Au@Ag)@Au double shell NPs loaded on TiO_2 is still not understood.

We synthesized (core@shell)@shell (Au@Ag)@Au NPs by a multistep citrate reduction method for utilization as photosensitizers of TiO_2 and successfully loaded them on rutile TiO_2 rods by an impregnation method. The rutile TiO_2 rods, which our previously synthesized through hydrothermal growth, showed high levels of activity for degradation of 2-propanol and acetaldehyde under UV irradiation compared to the activity levels of anatase fine particles (ST-01) developed by Ishihara sangyo Co. Ltd. [26]. The (Au@Ag)@Au/TiO_2 exhibited photocatalytic activity for decomposition of 2-propanol under visible light irradiation ($\lambda > 440$ nm), and its photocatalytic reaction rate was approximately 15-times higher than that of Au/TiO_2. In this paper, we present the photoctalytic activity of (Au@Ag)@Au/TiO_2 and discuss its photocatalytic reaction process in conjunction with optical, structural and photoelectrochemical properties.

2. Experimental

2.1. Preparation of (Au@Ag)@Au NPs and rutile TiO_2

(Au@Ag)@Au NPs were synthesized by a multistep citrate reduction method as follows (refer to Scheme 1). First, Au NPs were prepared for use as seeds for the synthesis of (Au@Ag)@Au NPs. Hydrogen tetrachloroaurate (III) tetrahydrate (99.0%, Wako Pure Chemical Industries Ltd.), trisodium citrate (99.0%, Wako Pure Chemical Industries Ltd.) and polyvinylpyrrolidone ($(C_6H_9NO)_n$; $n = 27\sim32$ Wako Pure Chemical Industries Ltd.) as starting reagents were mixed together thoroughly in distilled water at 70 °C. The mixed solution was stirred for 1 h and cooled to room temperature. The obtained suspension of Au NPs was a dark reddish color with an LSPR band at 522 nm, and average diameter of the Au NPs was 9 nm (Supporting information Fig. S1). Next, an Ag shell was grown on the Au seeds via seed-mediated growth for (core@shell) Au@Ag NPs. The obtained suspension of Au NPs was heated to reflux and then silver nitrate (99.5%, Wako Pure Chemical Industries Ltd.) and trisodium citrate were simultaneously added. After refluxing for 30 min, the outermost Au shell was grown on the Au@Ag NPs by adding hydrogen tetrachloroaurate (III) tetrahydrate and trisodium citrate solution. The mixed solution was refluxed for 30 min and cooled to room temperature. Then (Au@Ag)@Au NPs were obtained.

Rutile TiO_2 crystals were synthesized by a hydrothermal method that we previously reported [26,27]. In the synthesis procedure, a chemical solution was put in a sealed Teflon-lined autoclave reactor containing 50 mL aqueous solution of titanium trichloride, sodium chloride and poly(vinyl pyrrolidone). The solutions were then put into a 180 °C oven for 10 h. The substrate was centrifuged and rinsed with deionized water and then dried in a vacuum oven. After hydrothermal treatment, the organic compounds that remained or were adsorbed on the surface of TiO_2 particles were removed by ultraviolet (UV) irradiation with a 500 W super-high-pressure mercury lamp (Ushio, SX-UI501UO) for 24 h. The particles were dried under reduced pressure at 60 °C for 6 h. Then rutile TiO_2 crystals were obtained.

2.2. Loading (Au@Ag)@Au NPs on rutile TiO_2

The (Au@Ag)@Au NPs were loaded on rutile TiO_2 by an impregnation method. The impregnation was carried out by the following procedures: firstly, UV light ($\lambda = 365$ nm, intensity; 3 mW/cm^2) was irradiated to rutile TiO_2 for 3 days to remove organic compounds that remained or were adsorbed on the surface of TiO_2. Next, rutile TiO_2 powder and colloidal (Au@Ag)@Au NPs were put into an egg plant-shaped flask. This mixed solution was dispersed by sonication for 10 min and then dried by using a rotary evaporator on a water bath. After evaporation, the residue was washed with

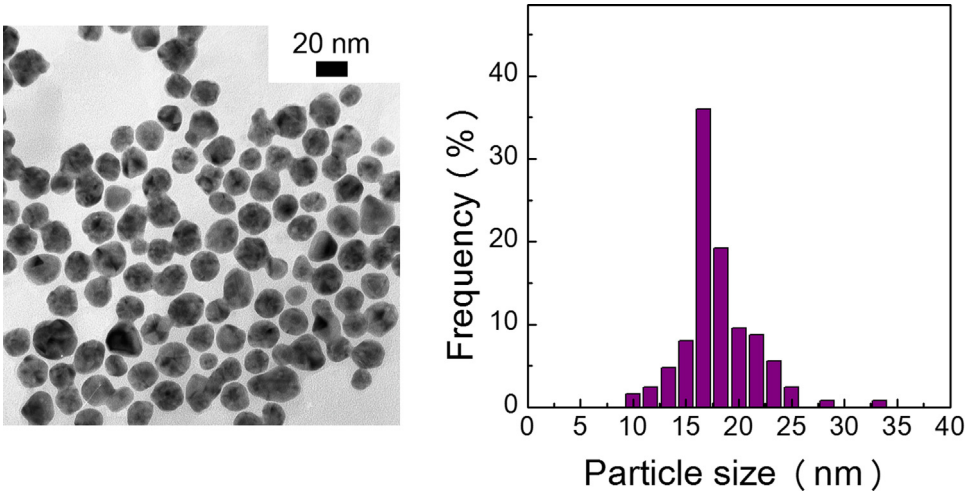

Fig. 1. TEM photograph (left) and size distributions (right) of colloidal (Au@Ag)Au NPs.

distilled water several times. Finally, the residual water was completely removed by using the vacuum freeze drying method. Then (Au@Ag)@Au/ TiO_2 was obtained. Au@Ag NPs and Au NPs were also loaded on rutile TiO_2 by the impregnation method as described above. It should be noted that amounts of loading of (Au@Ag)@Au NPs, Au@Ag NPs and Au NPs on TiO_2 were optimized at 0.75 wt.% (Supporting information Fig. S2).

2.3. Characterization

The (Au@Ag)@Au NPs were characterized by using a field emission high-resolution transmission electron microscope (HR-TEM; Tecnai G2 F30 S-TWIN, FEI) with a high-angle annular dark-field (STEM-HAADF) detector and by energy-dispersive X-ray spectroscopy (EDS) elemental mapping. An absorption spectrum of colloidal (Au@Ag)@Au NPs was acquired at room temperature with a UV–vis spectrometer (UV-2600, Shimadzu Co.). The crystalline phase of rutile TiO_2 was characterized by using a powder X-ray diffraction (XRD) instrument (MiniFlex II, Rigaku Co.) with CuKα (λ = 1.5418 Å) radiation (cathode voltage: 30 kV, current: 15 mA). A diffuse reflectance spectrum was acquired at room temperature with a UV/VIS spectrometer (UV-2600, Shimadzu Co.) attached to an integral sphere. X-ray photoelectron spectroscopy (XPS) measurements were performed using a Kratos AXIS Nova spectrometer (Shimazu Co.) with a monochromatic Al Kα X-ray source. The binding energy was calibrated by taking the carbon (C) 1s peak of contaminant carbon as a reference at 248.7 eV.

2.4. Photocatalytic decomposition of 2-propanol

Photocatalytic activity of (Au@Ag)@Au/TiO_2 was evaluated by photocatalytic decomposition of 2-propanol. Sample powder (0.16 mg) was spread on a glass dish (4.0 cm^2) and placed in a Tedlar bag (AS ONE Co. Ltd.) with a volume of 125 cm^3. The Tedlar bag was sealed by laminating after placement of the glass dish, and then 500 ppm of gaseous 2-propanol was injected into the Tedlar bag, in which gaseous composition was 79% N_2, 21% O_2, <0.1 ppm of CO_2 and 500 ppm of 2-propanol. After 2-propanol had reached an absorption equilibrium (after 2 h), the sample was irradiated with visible light at room temperature. A 500-W xenon lamp (Ushio, SX-UI501XQ) was used as a light source, and the wavelength of photoirradiation was controlled by a yellow-44 cut-off

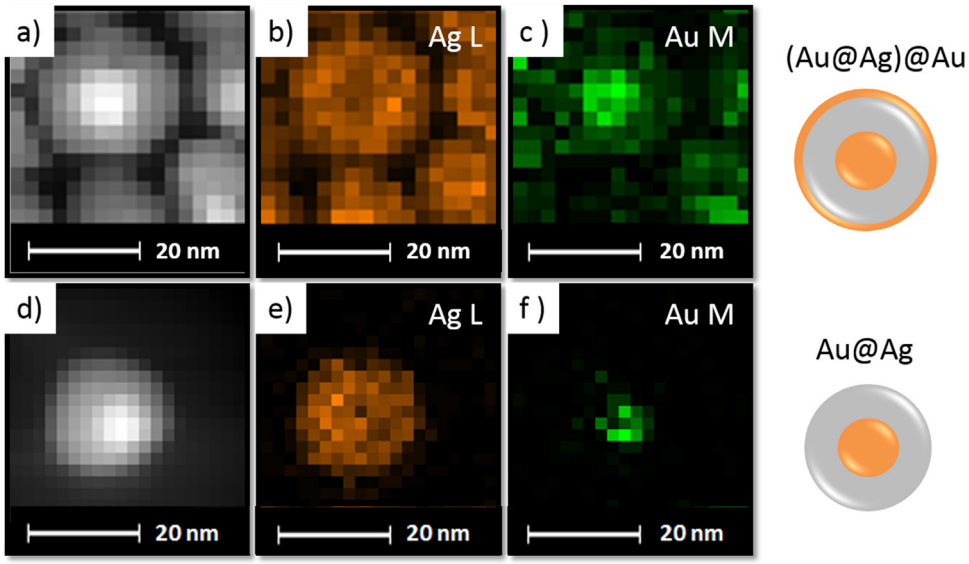

Fig. 2. STEM-HAADF image (a) and EDS elemental mapping for Ag L map (b), Au M map (c) of (Au@Ag)@Au NPs. The below images are for Au@Ag NPs with STEM-HAADF image (d) and EDS elemental mapping for Ag L map (e), Au M map (f).

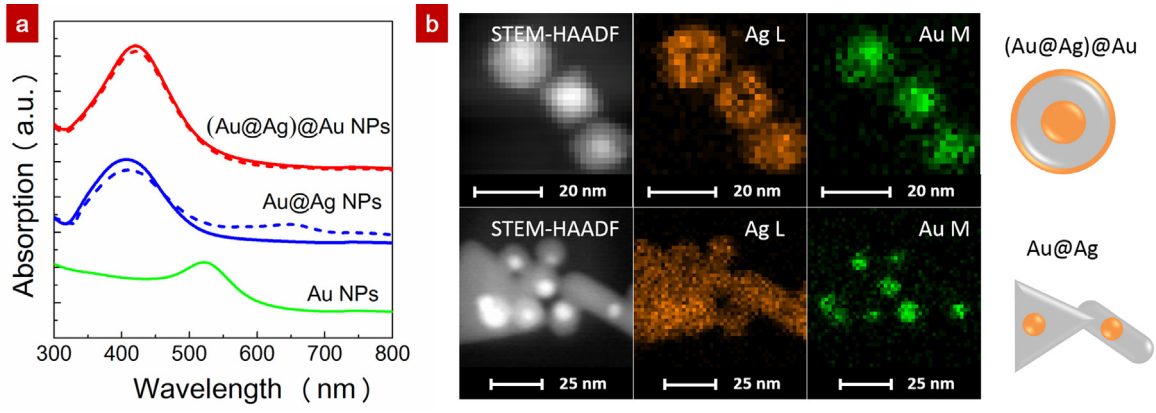

Fig. 3. (a) Absorption spectrum of colloidal (Au@Ag)@Au NPs, Au@Ag NPs and Au NPs, where solid lines are as prepared NPs and broken lines are after exposure to Xe lamp equipped with yellow-44 cut-off filter ($\lambda > 440$ nm, intensity = 30 mW/cm^2) for 72 h. (b) STEM-HAADF and EDS elemental mapping images between (Au@Ag)@Au NPs (top) and Au@Ag NPs (bottom) after exposure to Xe lamp for 72 h ($\lambda > 440$ nm, intensity = 30 mW/cm^2).

filter ($\lambda > 440$ nm, Asahi Techno Glass Co.). The intensity of light was adjusted to 30 mW/cm^2. The concentrations of 2-propanol, acetone and carbon dioxide (CO_2) were estimated by gas chromatography (Shimadzu, GC-8A, FID detector) with a PEG-20 M 20% Celite 545 packed glass column and by gas chromatography (Shimadzu, GC-9A, FID detector) with a TCP 20% Uniport R packed column and methanizer (GL Sciences, MT-221). Apparent quantum efficiency (AQE) at each wavelength was calculated from the ratio of the amount of acetone and the amount of incident photons. Light-emitting diodes was used as the light source peaking at 455 nm, 470 nm, 505 nm, 530 nm, 625 nm, and 720 nm (light intensity was adjusted at 1.0 mW/cm^2).

2.5. Photoelectrochemical measurements

Photoelectrochemical measurement was carried out by using an electrochemical analyzer (604D, ALS Co.) with a three–electrode system, wherethe (Au@Ag)@Au/TiO_2electrode, platinum, and silver-silver chloride (Ag/AgCl) were used as a working electrode, counter electrode, and reference electrode, respectively. The electrolyte was non-bubbled 0.1 M NaOH solution and its potential hydrogen (pH) was pH 14. The light source used was an Xe lamp equipped with yellow-44 cut-off filter ($\lambda > 440$ nm, Asahi Techno Glass Co.). The light intensity was determined to be 50 mW/cm^2 by utilizing a thermopile power meter (ORION-TH). The (Au@Ag)@Au/TiO_2 electrode was fabricated on fluorine-doped tin oxide (FTO) glass by the following procedure. Firstly, a rutile TiO_2 powder was deposited on the FTO glass in acetone solution by an electrophoretic method. After deposition of the rutile TiO_2 layer, (Au@Ag)@Au NPs were also deposited on the TiO_2/FTO glass in distilled water by the electrophoretic method.

3. Results and discussion

3.1. Characterization of (Au@Ag)@Au NPs

Fig. 1 shows a TEM photograph and distribution of colloidal (Au@Ag)@Au NPs. (Au@Ag)@Au NPs had an average particle size of 18.0 nm within a relatively sharp distribution with standard deviation of 2.8 nm. Fig. 2(a) shows a STEM-HAADF image of (Au@Ag)@Au NPs. Since the intensity (brightness) is approximately proportional to the square of the atomic number (Z^2) in a STEM-HAADF image, heavier Au atoms (atomic number: $Z = 79$) give rise to a brighter image than do lighter Ag atoms ($Z = 47$). This image indicates that core Au was covered by an Ag shell in (Au@Ag)@Au NPs. To investigate the outermost Au shell in (Au@Ag)@Au NPs,

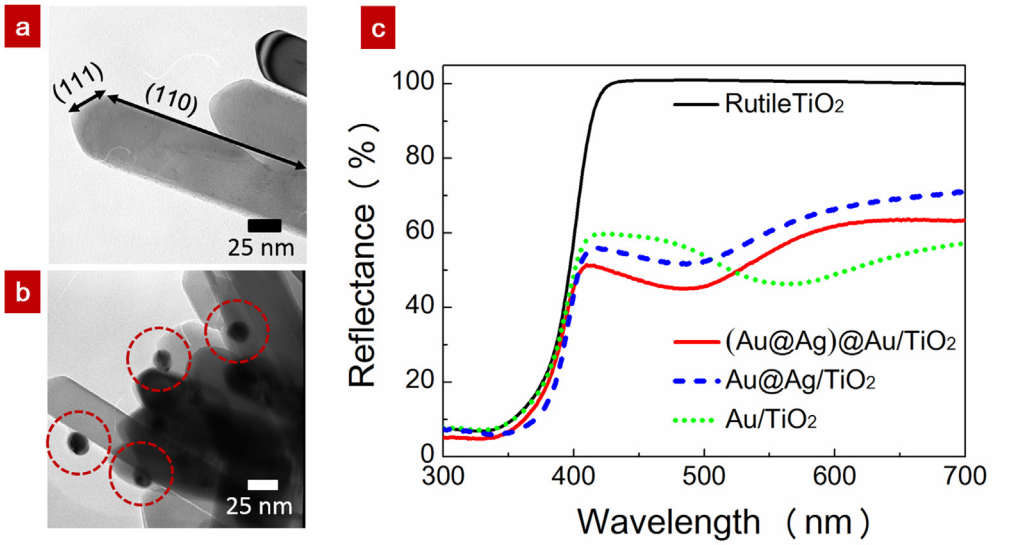

Fig. 4. (a) TEM photograph of rutile TiO_2 and (b) (Au@Ag)Au NPs loaded rutile TiO_2 (bottom). (c) Diffuse reflection spectrum of 0.75 w% (Au@Ag)@Au/TiO_2, 0.75 w% Au@Ag/TiO_2, 0.75 w% Au/TiO_2, and bare rutile TiO_2.

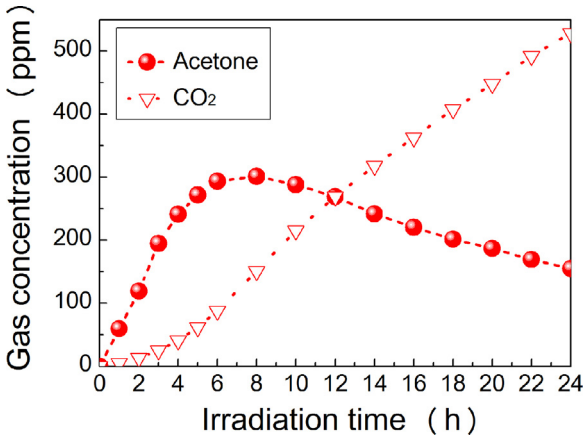

Fig. 5. Time course of acetone (solid circle) and CO_2 (open triangle) evolution of 2-propanol decomposition over 0.75 wt% (Au@Ag)Au/TiO_2 under irradiation of Xe lamp equipped with yellow-44 cut-off filter ($\lambda > 440$ nm, intensity = 30 mW/cm^2).

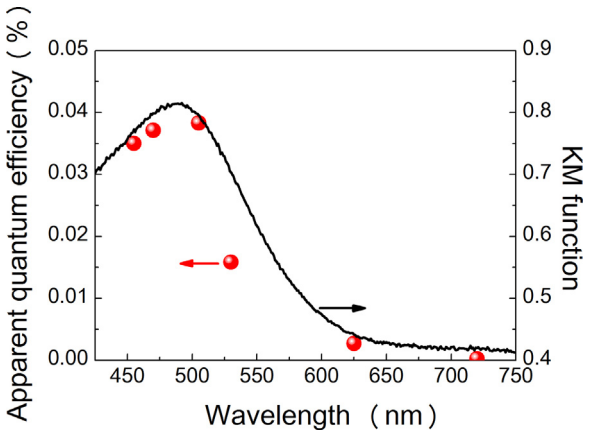

Fig. 6. Action spectrum (solid circle) of acetone evolution of 2-propanol decomposition over (Au@Ag)Au/TiO_2 (left axis) and the Kubelka–Munk function (solid line) of (Au@Ag)Au/TiO_2 (right axis).

EDS elemental mapping was performed. Data acquisition with high resolution was difficult due to sample drift, and we therefore compared EDS elemental mapping between (Au@Ag)@Au NPs and Au@Ag NPs to clarify the outermost Au shell. As shown in Fig. 2(b), (c), (e) and (f), the distribution of the Au M edge of Au@Ag NPs was located at only the center of particles. On the other hand, the distribution of the Au M edge of (Au@Ag)@Au NPs was spread around the particles, suggesting that an outermost Au shell could be formed in (Au@Ag)@Au NPs.

For utilization of (Au@Ag)@Au NPs as photosensitizers of TiO_2, visible-light response and stability are required. We investigated LSPR characteristics of colloidal (Au@Ag)@Au NPs before and after exposure to a Xe lamp equipped with a yellow-44 cut-off filter ($\lambda > 440$ nm). Fig. 3 shows an absorption spectrum of colloidal (Au@Ag)@Au NPs together with absorption spectra of Au@Ag NPs and Au NPs in aqueous solutions. Before exposure to the Xe lamp, colloidal (Au@Ag)@Au NPs exhibited strong absorption peaks centered at 420 nm. This peak was considered to be due to LSPR excitation of Ag. The appearance of a monomodal LSPR band corresponding to Ag indicates that the Au cores are uniformly covered by the Ag shell and the optical contribution from the Au cores is completely screened [24]. After exposure to the Xe lamp for 72 h, the absorption spectrum of (Au@Ag)@Au NPs was barely changed, implying that (Au@Ag)@Au NPs were stable under visible light irradiation for a long time.

On the other hand, the absorption spectrum of Au@Ag NPs changed after exposure to the Xe lamp; LSPR peak (λ_{max} = 407 nm) intensity was decreased and an additional LSPR peak centered at 650 nm was observed. A similar phenomenon was reported by Mirkin et al. who found a decrease in LSPR peak intensity of colloidal Ag NPs (λ_{max} = 400 nm) with a concomitant increase in LSPR peak intensity at 670 nm under 40 W fluorescent lamp illumination [28]. They revealed that fluorescent lamp irradiation for colloidal Ag NPs led to a change in morphology, resulting in a change in LSPR characteristics. As shown in Fig. 3, STEM-HAADF and the EDS elemental mapping images indicated that the degradation of the absorption spectrum of Au@Ag must be due to a change in the morphology of the Ag shell (see Fig. 3(b)). Wu et al. revealed that morphological conversions of Ag NPs were caused by coupling of the photo-oxidative dissolution and the subsequent photoreduction of aqueous Ag^+ ions [29]. Therefore, it is highly possible that the Ag shell in Au@Ag NPs was oxidized by visible light irradiation, leading to morphological conversions, which resultted in a decrease of absorption intensity and a change in the absorption spectrum. In contrast, LSPR characteristics of (Au@Ag)@Au NPs were stable under visible light irradiation for a long time because oxidation of the Ag shell may be prevented by the outermost Au shell.

3.2. Characterization of (Au@Ag)@Au NPs/TiO_2

Fig. 4(a) shows a TEM photograph of rutile TiO_2. Rod-like morphology was confirmed and most of the rutile rods consisted of flat side surfaces and triangular-like caps, similar to the structure reported for rutile rods with {110} and {111} exposed crystal faces and longer length along the [001] direction [26,27,30]. Fig. 4(b) shows a TEM photograph of rutile TiO_2 with (Au@Ag)@Au NPs. Small (Au@Ag)@Au NPs were observed and their average diameter was determined to be ca. 19 nm, indicating that (Au@Ag)@Au NPs were successfully loaded on the surface of rutile TiO_2 by the impregnation method.

Fig. 4(c) shows a diffuse reflection spectrum of (Au@Ag)@Au/TiO_2 together with diffuse reflection spectra of bare rutile TiO_2, Au/TiO_2 and Au@Ag/TiO_2. The bare rutile TiO_2 exhibited only strong photoabsorption at $\lambda < 400$ nm, which was ascribed to the band-gap excitation. In the case of Au/TiO_2, an additional absorption peak was observed at around 560 nm. Kowalska et al. reported that photoabsorption of Au NPs loaded on rutile TiO_2 was observed at around 550 nm due to thier LSPR excitation. Therefore, photoabsorption observed in Au/TiO_2 was attributed to LSPR excitation of the loaded Au NPs. (Au@Ag)@Au NPs and Au@Ag NPs loaded on rutile TiO_2 exhibited strong absorption peaks centered at 484 nm and 486 nm, respectively. These absorption peaks were ascribed to LSPR excitation of the Ag shell in loaded (Au@Ag)@Au NPs and Au@Ag NPs on the basis of the absorption spectra of colloidal (Au@Ag)@Au NPs and Au@Ag NPs (refer to Fig. 3).

3.3. Photocatalytic activities

Photocatalytic activity was evaluated by oxidation of 2-propanol in gas phase. Fig. 5 shows the time course of acetone and CO_2 evolution from decomposition of 2-propanol over (Au@Ag)@Au/TiO_2 under irradiation by an Xe lamp equipped with a yellow-44 cut-off filter ($\lambda > 440$ nm, 30 mW/cm^2). Acetone evolution increased almost linearly with irradiation time up to 6 h, and followed by a gradually decrease with irradiation time due to accumulation of acetone on the surface of (Au@Ag)@Au/TiO_2. After prolonged visible light irradiation, the acetone was finally decomposed into CO_2. This behavior is plausible as it is known that 2-propanol decomposes into CO_2, which is the final product, via acetone, the intermediary product [31–33]. It should be noted that acetone and CO_2 were not

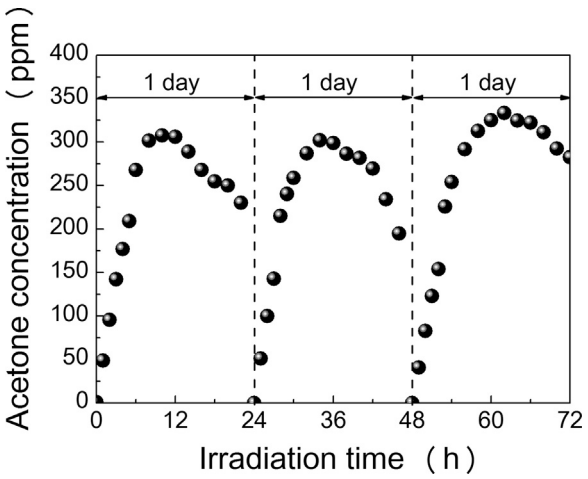

Fig. 7. Time course of acetone evolution of 2-propanol decomposition over the (Au@Ag)Au/TiO_2 (solid circle) under visible light irradiation for 24 h (Xe lamp, λ > 440 nm) which measured up to 3 cycles. After 24 and 48 h irradiation, residual gas was evacuated and additional 2-propanol (500 ppm) was injected followed by irradiated again.

detected under dark conditions or under visible light irradiation in the absence of (Au@Ag)@Au/TiO_2.

An action spectrum is a strong tool for determining whether a reaction observed in (Au@Ag)@Au/TiO_2 occurs via a photo-induced process or a thermocatalytic process. To obtain an action spectrum, acetone evolution from decomposition of 2-propanol over (Au@Ag)@Au/TiO_2 was measured at room temperature under visible light irradiation by using light-emitting diodes peaking at 455 nm, 470 nm, 505 nm, 530 nm, 625 nm and 720 nm, respectively. Apparent quantum efficiency (AQE) at each wavelength was calculated from the ratio of the amount of acetone and the amount of incident photons using the following equation:

$$\mathrm{AQE} = \frac{\text{amount of acetone molecules} \times 2}{\text{amount of incident photons}}$$

As shown in Fig. 6, AQE was in good agreement with the Kubelka–Munk function of (Au@Ag)@Au/TiO_2, indicating that photocatalytic activity of (Au@Ag)@Au/TiO_2 was induced by photoabsorption based on LSPR excitation of the Ag shell. Fig. 7 shows the results of cycle tests of acetone evolution from decomposition of 2-propanol over (Au@Ag)@Au/TiO_2 under irradiation by an Xe lamp equipped with a yellow-44 cut-off filter (λ > 440 nm, 30 mW/cm^2). In the first cycle, acetone evolution increased almost linearly with irradiation time followed by a gradual decrease with irradiation time as described above. After 24 h and 48 h of irradiation, residual acetone was removed by evacuation and additional 2-propanol was injected followed by irradiation again. As in the first cycle, acetone evolution increased with irradiation time, indicating that (Au@Ag)@Au/TiO_2 continuously decomposed 2-propanol under visible light irradiation without losing its activity.

Thus, (Au@Ag)@Au/TiO_2 can oxidize 2-propanol into acetone and CO_2 under visible light irradiation (λ > 440 nm), and its activity is attributed to LSPR excitation of the Ag shell. Therefore, we calculated the turnover number of the Ag shell in loaded (Au@Ag)@Au NPs. The present sample (0.75 wt.% (Au@Ag)@Au/TiO_2) contained ca. 8.8 μmol Ag, and CO_2 evolution was confirmed to be ca. 2.7 μmol after irradiation for 24 h (see Fig. 4). Assuming that six photons are required to produce one CO_2 molecule, as follows:

$$(CH_3)_2CHOH + 5H_2O + 18h^+ \rightarrow 3CO_2 + 18H^+$$

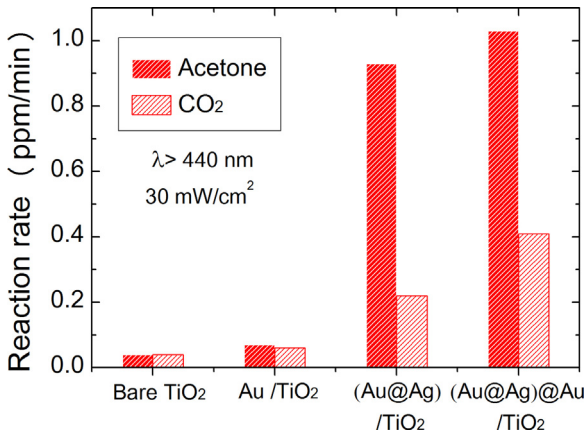

Fig. 8. Acetone and CO_2 evolution rates of 2-propanol decomposition over the f 0.75 w% (Au@Ag)@Au/TiO_2, 0.75 w% Au@Ag/TiO_2, 0.75 w% Au/TiO_2, and bare rutile TiO_2 under visible light irradiation (λ > 440 nm).

The turnover number of the Ag shell in (Au@Ag)@Au NPs was more than ca. 1.84, which is enough to prove that the reaction observed was a photocatalytic reaction.

Fig. 8 shows a comparison of acetone and CO_2 evolution rates of (Au@Ag)@Au/TiO_2, Au@Ag/TiO_2, Au/TiO_2 and bare rutile TiO_2 under irradiation by a Xe lamp equipped with yellow-44 cut-off filter (λ > 440 nm, 30 mW/cm^2). As shown in this figure, acetone and CO_2 evolution rates increased in the order of bare TiO_2 < Au/TiO_2 « Au@Ag/TiO_2 < (Au@Ag)@Au/TiO_2, implying that LSPR excitation of Ag could produce higher photocatalytic activity than that of Au. Shiraishi and colleagues suggested that Schottky barrier height at Au/TiO_2 junction was much larger than that of AuAg/TiO_2 [34]. We presumed that electron injection from LSPR-excited Au@Ag NPs to TiO_2 has effectively occurred, thereby Au@Ag/TiO_2 shows much enhanced activity as compared to Au/TiO_2. The electron injection process from LSPR-excited (Au@Ag)@Au NPs to TiO_2 will be discussed later based on photoelectrochemical properties.

The acetone evolution rate of Au@Ag/TiO_2 was same as that of (Au@Ag)@Au/TiO_2, while the CO_2 evolution rate of Au@Ag/TiO_2 was smaller than that of (Au@Ag)@Au/TiO_2 (time course data was presented in Supporting information Fig. S3). To clarify this phenomenon, XPS measurement was done before and after photocatalytic activity tests for decomposition of 2-propanol, and the Ag *3d* spectra are shown in Fig. 9. Before exposure to an Xe lamp (λ > 440 nm), both of the samples exhibited two sharp peaks at

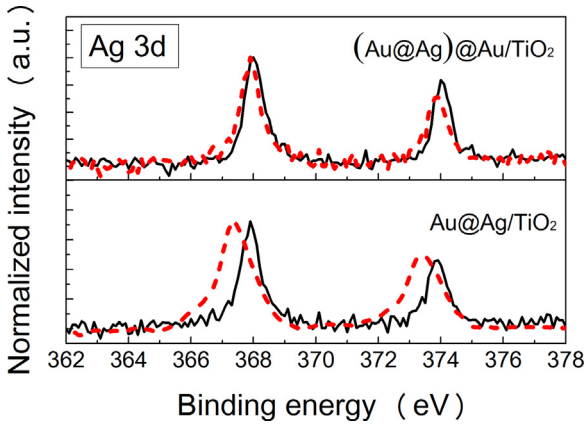

Fig. 9. XPS spectra of Ag *3d* of (Au@Ag)@Au/TiO_2 and Au@Ag/TiO_2 before (solid lines) and after (broken lines) photocatalytic activity tests for decomposition of 2-propanol.

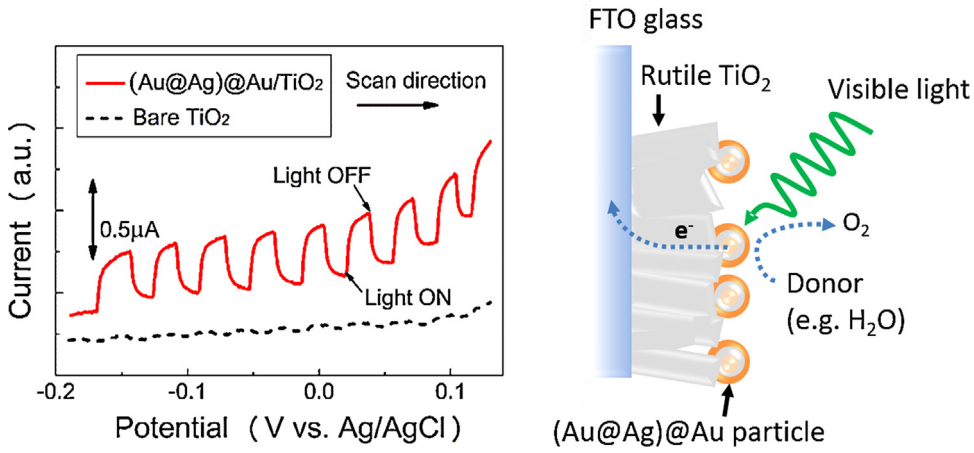

Fig. 10. Linear sweep voltammetry of (Au@Ag)@Au/TiO_2 and bare TiO_2 electrode under "chopped" Xe lamp irradiation ($\lambda > 440$ nm). The electrolyte is non-bubbled aqueous NaOH solution (pH 14). Right figure is expected working mechanism of anodic photocurrent from (Au@Ag)Au/TiO_2 electrode under visible light irradiation.

367.9 eV and 374 eV, which were attributed to typical values of Ag $3d_{5/2}$ and $3d_{3/2}$, respectively. After photoirradiation, the Ag *3d* XPS spectrum of Au@Ag/TiO_2 shifted to lower binding energy, with peaks at 367.4 eV and 373.4 eV, respectively. These peaks were identified to be silver oxide AgO [35], indicating that Au@Ag NPs were oxidized by irradiation of visible light. Sukhishvili et al. revealed that oxidation of the surfaces of Ag NPs hinders charge transfer between Ag and organic molecules [36]. Therefore, we speculated that oxidation of Au@Ag NPs on TiO_2 suppressed photocatalytic oxidation of acetone under photoirradiation for a long time, resulting in a lower rate of CO_2 evolution than that with (Au@Ag)@Au/TiO_2.

3.4. Photoelectrochemical properties

There have been several reports concerning the mechanism of LSPR-induced photocatalytic reaction of Au NPs/TiO_2 [14–16]. Electron injection from LSPR-excited Au NPs to TiO_2 and subsequent oxidation of 2-propanol at Au NPs have been proposed as for the reaction mechanism. Actually, Furube et al. observed electron transfer from excited Au NPs to TiO_2 particles by means of femtosecond transient absorption spectroscopy [16].

Photoelectrochemical measurement was done to clarify the electron transfer process of (Au@Ag)@Au/TiO_2. Fig. 10 shows linear sweep voltammetry of the (Au@Ag)@Au/TiO_2 electrode in 0.1 M NaOH solution with irradiation of visible light ($\lambda > 440$ nm) together with that of the rutile TiO_2 electrode. As clearly shown in this figure, the (Au@Ag)@Au/TiO_2 photoelectrode exhibited an anodic photocurrent in response to irradiation of visible light, and the anodic photocurrent density reached 0.1 $\mu A/cm^2$ at 0 V applied potential versus Ag/AgCl. In contrast, the bare rutile TiO_2 electrode did not exhibit an anodic photocurrent under visible light. It should be noted that Au@Ag/TiO_2 electrode was not necessarily stable during photoelectrochemical measurement, thereby photocurrent could not be detected (Supporting information Fig. S4). These photoresponse results indicated that electron transfer from LSPR-excited (Au@Ag)@Au NPs to rutile TiO_2 occurred with subsequent oxidation of water at (Au@Ag)@Au NPs.

On the basis of the above results, we proposed the following reaction process for the photocatalytic decomposition of 2-propanol over (Au@Ag)@Au/TiO_2: (1) when visible light was irradiated to the (Au@Ag)@Au/TiO_2, photons are absorbed by the (Au@Ag)@Au NPs due to LSPR excitation of middle Ag shell, as was proved by action spectrum analysis, (2) the excited electrons in the (Au@Ag)@Au NPs are injected into the conduction band of rutile TiO_2, and then the electron-deficient (Au@Ag)@Au NPs can oxidize 2-propanol into acetone and CO_2, and (3) the resultant electron-deficient (Au@Ag)@Au NPs recovers original state.

4. Conclusions

Colloidal (core@shell)@shell ((Au@Ag)@Au) NPs were synthesized and successfully loaded on rutile TiO_2 by using an impregnation method. The (Au@Ag)@Au NPs loaded on TiO_2 showed strong photoabsorption at around 420 nm due to LSPR of the Ag shell, and its LSPR characteristics were stable under visible light irradiation for a long time because oxidation of the Ag shell was prevented by the outermost Au shell. Furthermore, we revealed that (Au@Ag)@Au NPs/TiO_2 can oxidize 2-propanol into acetone and CO_2 under visible light irradiation ($\lambda > 440$ nm) and that the acetone generation rate of (Au@Ag)@Au NPs/TiO_2 was approximately 15-times higher than that of Au NPs/TiO_2. From a comparison of action spectra for acetone evolution and the Kubelka-Munk function, it was confirmed that photocatalytic activity of (Au@Ag)@Au/TiO_2 was induced by photoabsorption based on LSPR excitation of the Ag shell. The turnover number of the Ag shell in (Au@Ag)@Au/TiO_2 was more than ca. 1.8, which is enough to prove that the reaction observed was photocatalytic reaction. Photoelectrochemical measurements revealed electron injection from LSPR excited (Au@Ag)@Au NPs into TiO_2 under visible light irradiation. We proposed the photocatalytic reaction process for (Au@Ag)@Au/TiO_2.

Acknowledgements

The authors thank to Prof. Tetsuya Haruyama, Prof. Yoichi Shimizu, and Prof. Naoya Murakami of Kyushu Institute of Technology, and Prof. Takeshi Fukuma of Kanazawa Univ. for their valuable contributions to this study. This work has been supported by a grant from Advanced Catalytic Transformation program for Carbon utilization (ACT-C), and Japan Science and Technology Agency (JST).

Appendix A. Supplementary data

Supplementary data associated with this article can be found, in the online version, at http://dx.doi.org/10.1016/j.apcatb.2015.06.037

References

[1] A. Fujishima, K. Honda, Nature 238 (1972) 37.
[2] M.R. Hoffmann, S.T. Martin, W. Choi, D.W. Bahnemann, Chem. Rev. 95 (1995) 69.
[3] K. Hashimoto, H. Irie, A. Fujishima, Jpn. J. Appl. Phys. 12 (2005) 8269.
[4] K. Nakata, A. Fujishima, J. Photochem. Photobiol. C 13 (2012) 169.
[5] S.N. Habisreutinger, L. Schmidt-Mende, J.K. Stolarczyk, Angew. Chem. Int. Ed. 52 (2013) 7372.
[6] Y.K. Kho, A. Iwase, W.Y. Teoh, L. Madler, A. Kudo, R. Ama, J. Phys. Chem. C 114 (2010) 2821.
[7] T. Ohno, M. Akiyoshi, T. Umebayashi, K. Asai, T. Mitsui, M. Matsumura, Appl. Catalysis A 265 (2004) 115.
[8] B. O'regan, M. Grätzel, Nature 353 (1991) 737.
[9] R. Asahi, T. Morikawa, T. Ohwaki, K. Aoki, Y. Taga, Science 293 (2001) 269.
[10] M. Grätzel, J. Photochem. Photobiol. A 164 (2004) 3.
[11] W. Choi, A. Termin, M.R. Hoffmann, J. Phys. Chem. 98 (1994) 13669.
[12] T. Wu, G. Liu, J. Zhao, J. Phys. Chem. B 102 (1998) 5845.
[13] Y. Zhao, J.R. Swierk, J.D. Megiatto Jr., B. Sherman, W.J. Youngblood, D. Qin, D.M. Lentz, A.L. Moore, T.A. Moore, D. Gust, T.E. Mallouk, Proc. Natl. Acad. Sci. U. S. A. 109 (2012) 15612.
[14] Y. Tian, T. Tatsuma, J. Am. Chem. Soc. 127 (2005) 7632.
[15] E. Kowalska, O.O.P. Mahaney, R. Abe, B. Ohtani, Phys. Chem. Chem. Phys. 12 (2010) 2344.
[16] A. Furube, L. Du, K. Hara, R. Katoh, M. Tachiya, J. Am. Chem. Soc. 129 (2007) 14852.
[17] K. Kimura, S. Naya, Y. Jin-nouchi, H. Tada, J. Phys. Chem. C 116 (2012) 7111.
[18] A. Tanaka, S. Sakaguchi, K. Hashimoto, H. Kominami, ACS Catal. 3 (2013) 79.
[19] F. Pincella, K. Isozaki, K. Miki, Light: Sci. Appl. 3 (2014) 1.
[20] Y. Tian, T. Tatsuma, Chem. Comm. (2004) 1810.
[21] A. Romanyuk, P. Oelhafen, Sol. Energy Mater. Sol. Cells 91 (2007) 1051.
[22] Y. Yin, Z.Y. Li, Z. Zhong, B. Gates, Y. Xia, S. Venkateswaranc, J. Mater. Chem. 12 (2002) 522.
[23] I. Tanabe, T. Tatsuma, Nano Lett. 12 (2012) 5418.
[24] D.T.N. Anh, P. Singh, C. Shankar, D. Mott, S. Maenosono, Appl. Phys. Lett. 99 (2011), 073107–1.
[25] S. Nishimura, A.T.N. Dao, D. Mott, K. Ebitani, S. Maenosono, J. Phys. Chem. C 116 (2012) 4511.
[26] E. Bae, N. Murakami, T. Ohno, J. Mol. Catal. A: Chem. 300 (2009) 72.
[27] K. Bae, T. Ohno, Appl. Catal. B 91 (2009) 634.
[28] R. Jin, Y.W. Cao, C.A. Mirkin, K.L. Kelly, G.C. Schatz, J.G. Zheng, Science 294 (2001) 1901.
[29] X. Wu, P.L. Redmond, H. Liu, Y. Chen, M. Steigerwald, L. Brus, J. Am. Chem. Soc. 130 (2008) 9500.
[30] K. Kakiuchi, E. Hosono, H. Imai, T. Kimura, S. Fujihara, J. Cryst. Growth 293 (2006) 541.
[31] Y. Ohko, K. Hashimoto, A. Fujishima, J. Phys. Chem. A 101 (1997) 8057.
[32] H. Yamashita, M. Honda, M. Harada, Y. Ichihashi, M. Anpo, J. Phys. Chem. B 102 (1998) 10707.
[33] H. Irie, S. Miura, K. Kamiya, K. Hashimoto, Chem. Phys. Lett. 457 (2008) 202.
[34] D. Tsukamoto, A. Shiro, Y. Shiraishi, Y. Sugano, S. Ichikawa, S. Tanaka, T. Hirai, ACS Catal. 2 (2012) 599.
[35] G.B. Hoflund, Z.F. Hazos, Phys. Rev. B 62 (2000) 126.
[36] M. Erol, Y. Han, S.K. Stanley, C.M. Stafford, H. Du, S. Sukhishvili, J. Am. Chem. Soc. 130 (2008) 9500.